Effective Wavelength Scaling for Optical Antennas

Lukas Novotny*

Institute of Optics, University of Rochester, Rochester, New York, USA

(Received 27 March 2007; published 27 June 2007)

In antenna theory, antenna parameters are directly related to the wavelength λ of incident radiation, but this scaling fails at optical frequencies where metals behave as strongly coupled plasmas. In this Letter we show that antenna designs can be transferred to the *optical* frequency regime by replacing λ by a linearly scaled effective wavelength $\lambda_{\text{eff}} = n_1 + n_2\lambda/\lambda_p$, with λ_p being the plasma wavelength and n_1, n_2 being coefficients that depend on geometry and material properties. It is assumed that the antenna is made of linear segments with radii $R \ll \lambda$. Optical antennas hold great promise for increasing the efficiency of photovoltaics, light-emitting devices, and optical sensors.

DOI: 10.1103/PhysRevLett.98.266802 PACS numbers: 73.20.Mf, 68.37.Uv, 78.67.−n, 84.40.Ba

In the radio frequency and microwave regimes antennas are widely employed to convert electromagnetic radiation into localized energy and *vice versa*. However, at *optical* frequencies, lenses and mirrors are used to redirect the wave fronts of propagating radiation and the antenna concept is widely unexplored [1]. Consequently, the best possible localization of optical radiation is governed by the diffraction limit.

The extension of the antenna concept into the optical wavelength range has many foreseeable applications, such as high-resolution microscopy and spectroscopy [2–5], optical sensors [6,7], photovoltaics [8,9], solid state lighting [10,11], and lasing [12]. The development of optical antennas demands design rules that make it possible to transfer established antenna designs from the radio wave to the optical frequency range. Recent theoretical and experimental studies have shown that the resonant length of optical dipole antennas is considerably shorter than one-half the wavelength of the incident light [7,12–14]. This is in contradiction to classical antenna theory and it is the objective of this Letter to explain and understand this phenomenon.

Traditional antenna design makes use of structures with characteristic lengths L that are directly related to the wavelength λ of the incoming (or outgoing) radiation, i.e., $L = \text{const} \times \lambda$, where const is an antenna-design constant. For example, an ideal half-wave dipole antenna is made of a thin rod of length $L = (1/2)\lambda$ [15]. However, at optical frequencies the simple wavelength scaling breaks down because incident radiation is no longer perfectly reflected from a metal's surface. Instead, radiation penetrates into the metal and gives rise to oscillations of the free-electron gas. Hence, at *optical* frequencies an antenna no longer responds to the external wavelength but to a shorter *effective* wavelength λ_{eff} which depends on the material properties. The necessity of replacing λ by a shorter effective wavelength is evident from recent experiments performed at infrared frequencies [16,17]. In these experiments the resonances of lithographically fabricated antennas turned out to be 20% shorter than the value predicted by antenna theory. An effective wavelength has been arrived at by taking the complex surface impedance of the metal into account [18]. However, when the length scales of the antenna (e.g., thickness of wires) become comparable with the skin depth of the metal the concept of the surface impedance breaks down and the electromagnetic response becomes dictated by collective electron oscillations characteristic of a strongly coupled plasma. For example, for a half-wave antenna made of a gold rod (length 110 nm, radius 5 nm) one calculates $\lambda_{\text{eff}} = \lambda/5.3$ ($L = \lambda/10.6$).

In this Letter we derive a simple linear scaling law for λ_{eff} in the form

$$\lambda_{\text{eff}} = n_1 + n_2[\lambda/\lambda_p], \tag{1}$$

where λ_p is the plasma wavelength and n_1, n_2 are coefficients with dimensions of length that depend on antenna geometry and static dielectric properties. The assumptions are that the antenna is made of linear segments with radius $R \ll \lambda$ and that the metal can be described by a free-electron gas according to the Drude model.

Figure 1 shows the parameters used in our model. We consider a single antenna segment (rod) with dielectric function $\varepsilon(\lambda)$, radius R, and total length L. The rod is embedded in a medium with dielectric constant ε_s and wave number $k_s = \sqrt{\varepsilon_s}2\pi/\lambda = \sqrt{\varepsilon_s}k_o$. We argue that an incident wave with wavelength λ polarizes the ends of the rod thereby giving rise to a surface charge wave propagating along the rod. According to this picture, the effective

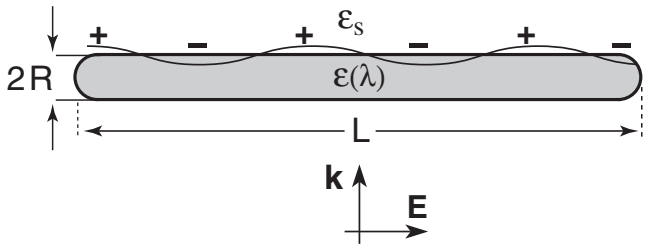

FIG. 1. A single antenna element represented by a metal rod. Incident light with wavelength λ polarizes the ends and gives rise to a standing surface charge wave.

wavelength is calculated as [19]

$$\lambda_{\text{eff}} = \lambda[k_o/\gamma] - 4R, \tag{2}$$

where $k_o = 2\pi/\lambda$ is the free-space wave number and γ is the propagation constant of the surface charge wave. The subtraction of $4R$ is approximate and originates from the apparent increase of the antenna length due to the reactance of the rod ends. Equation (2) states that the ratio $\lambda_{\text{eff}}/\lambda$ scales as the ratio k_o/γ, which is known as the *velocity factor* in antenna theory.

To determine γ it is necessary to calculate the modes of a thin metal wire. According to waveguide theory, the TM_0 modes of a cylindrical waveguide are solutions of

$$\frac{\varepsilon(\lambda)}{\kappa_1 R}\frac{J_1(\kappa_1 R)}{J_0(\kappa_1 R)} - \frac{\varepsilon_s}{\kappa_2 R}\frac{H_1^{(1)}(\kappa_2 R)}{H_0^{(1)}(\kappa_2 R)} = 0. \tag{3}$$

Here, J_n are cylindrical Bessel functions and $H_n^{(1)}$ are cylindrical Hankel functions of the first kind. The transverse wave numbers κ_1 and κ_2 are defined by the propagation constant γ as $\kappa_1 = k_o[\varepsilon - (\gamma/k_o)^2]^{1/2}$ and $\kappa_2 = k_o[\varepsilon_s - (\gamma/k_o)^2]^{1/2}$, respectively. We are interested in the spectral (dispersive) properties of the antenna response and therefore replace the dielectric constant ε by its real part $\varepsilon' = \text{Re}\{\varepsilon\}$.

For thin wires, J_n and $H_n^{(1)}$ can be expanded to first order in $\kappa_i R$ [20] and Eq. (3) reduces to

$$\frac{1}{(\kappa_2 R)^2} + A\frac{\varepsilon'}{2\varepsilon_s} + \left[\frac{2A - 2A^2 - 1}{4A}\right] = 0, \tag{4}$$

where $A(\kappa_2 R) = \Gamma - \ln(2) + \ln|\kappa_2 R|$ and $\Gamma = 0.577\ldots$ is the Euler constant. We now introduce the substitution

$$z = \sqrt{-\frac{2\varepsilon_s}{\varepsilon'}}\frac{1}{k_s R}\frac{(k_s/\gamma)}{[1 - (k_s/\gamma)^2]^{1/2}}, \tag{5}$$

which allows us to express Eq. (4) as

$$z^2 + A(z) + \frac{2\varepsilon_s}{\varepsilon'}\left[\frac{2A - 2A^2 - 1}{4A}\right] = 0. \tag{6}$$

For long wavelengths λ the dielectric constant ε increases much faster than the expression in brackets. Therefore, we expand the latter in powers of $(z - 1)$ and obtain to lowest order

$$\left[\frac{2A - 2A^2 - 1}{4A}\right] \approx \left[\frac{2A_o - 2A_o^2 - 1}{4A_o}\right] = B_o(\lambda), \tag{7}$$

where $A_o = \Gamma - (1/2)\ln[-2\varepsilon'/\varepsilon_s]$. The second term in Eq. (6) can be expanded to second order in $(z - 1)$ and becomes $A(z) \approx A_o - [(z - 1) - (1/2)(z - 1)^2]$. Equation (6) can now be solved for z and yields

$$z(\lambda) = \tfrac{2}{3} + \tfrac{1}{3}\sqrt{3\ln(-2\varepsilon'/\varepsilon_s) - 12B_o(\varepsilon_s/\varepsilon') - 6\Gamma - 5}. \tag{8}$$

To proceed, we consider a rod characterized by a free-electron gas according to the Drude formula

$$\varepsilon'(\lambda) = \varepsilon_\infty - \lambda^2/\lambda_p^2. \tag{9}$$

Here, $\varepsilon_\infty = \varepsilon'(\lambda \to 0)$ is the infinite frequency limit of the dielectric function, and λ_p is the plasma wavelength. For gold $\varepsilon_\infty \approx 11$, $\lambda_p \approx 138$ nm, and for silver $\varepsilon_\infty \approx 3.5$, $\lambda_p \approx 135$ nm. After inserting ε' defined in Eq. (9) into Eq. (8) we expand $z(\lambda)$ into a series around $\lambda = \lambda_p[\varepsilon_\infty + (\varepsilon_s/2)\exp(2\zeta)]^{1/2}$, where $\zeta = (5/3 + 2\Gamma)$. After a few arrangements and approximations we find

$$z(\lambda)\sqrt{\frac{-\varepsilon'}{2\varepsilon_s}} = \frac{\lambda}{\lambda_p}\frac{2\sqrt{\varepsilon_\infty + \varepsilon_s e^{2\zeta}/2}}{3\varepsilon_s e^{\zeta}}\left[1 + \frac{\sqrt{3}}{2}\frac{1+\zeta}{\sqrt{\zeta}}\right] + \frac{1}{3}e^{\zeta}\left[1 + \frac{\sqrt{3\zeta}}{2}\right] - \frac{2[\varepsilon_\infty + \varepsilon_s e^{2\zeta}/2]}{3\varepsilon_s e^{\zeta}}\left[1 + \frac{\sqrt{3}}{2}\frac{1+\zeta}{\sqrt{\zeta}}\right] \equiv a_1 + a_2\lambda/\lambda_p = \tilde{z}(\lambda). \tag{10}$$

We have suppressed higher order terms in λ because they are negligibly small.

The solution for $z(\lambda)$ can be inserted into Eq. (5) which yields the solution

$$\frac{k_s}{\gamma} = \left[\frac{(k_s R)^2\tilde{z}^2}{1 + (k_s R)^2\tilde{z}^2}\right]^{1/2}. \tag{11}$$

The effective wavelength is now calculated as

$$\lambda_{\text{eff}} = \frac{\lambda}{\sqrt{\varepsilon_s}}\sqrt{\frac{4\pi^2\varepsilon_s(R^2/\lambda^2)\tilde{z}(\lambda)^2}{1 + 4\pi^2\varepsilon_s(R^2/\lambda^2)\tilde{z}(\lambda)^2}} - 4R, \tag{12}$$

where $\tilde{z}(\lambda)$ is defined by Eq. (10). This equation represents a straightforward wavelength scaling and is the main result of this Letter. For a perfectly conducting material of negligible thickness ($R \to 0$) we obtain $\lambda_{\text{eff}} = \lambda$, in agreement with antenna theory. The expression defined by the square root scales as $a + b/\lambda$, with a and b being coefficients that depend on R and material parameters. We thus recover the simple linear relationship stated earlier in Eq. (1).

The linear wavelength scaling is also reproduced by numerically solving Eq. (3) and using experimental data for the dielectric function $\varepsilon(\lambda)$. Figure 2 shows the results for different rod radii R and for different materials. The linear relationship between λ and λ_{eff} is evident in all cases. Because of interband transitions one observes a slight deviation near $\lambda \approx 500$ nm for gold and near $\lambda \approx 800$ nm for aluminum.

For sufficiently small R the square root in Eq. (12) can be expanded using $\sqrt{x/(1+x)} \approx \sqrt{x}$ and yields

$$\lambda_{\text{eff}} = 2\pi R(a_1 + a_2\lambda/\lambda_p) - 4R, \tag{13}$$

where a_1 and a_2 were defined in Eq. (10). Numerical evaluation of a_1 and a_2 leads to

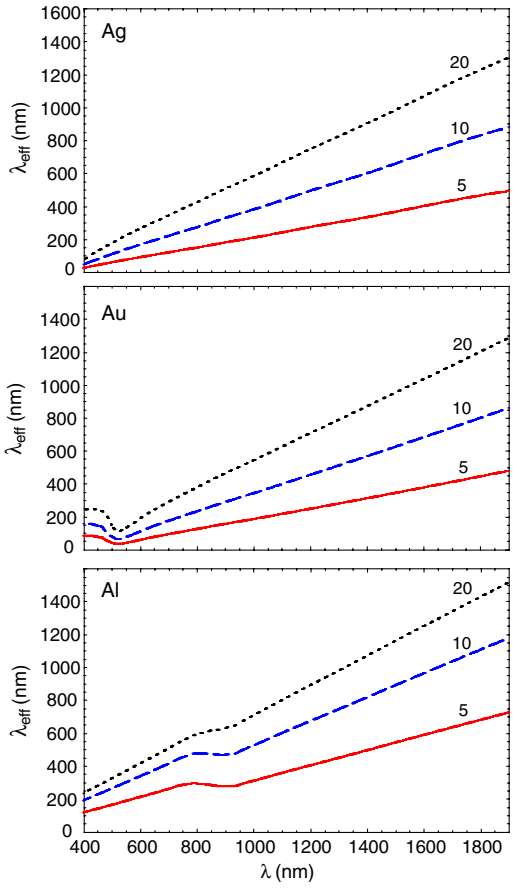

FIG. 2 (color online). Effective wavelength for metal rods made of silver, gold, and aluminum. The curves are calculated according to $\lambda_{\text{eff}} = \lambda(k_o/\gamma) - 4R$, where R is the wire radius and (k_o/γ) is determined numerically according to Eq. (3). Experimental values for $\varepsilon(\lambda)$ are used [25,26]. The rods are surrounded by vacuum ($\varepsilon_s = 1$). The numbers in the figures indicate the radius R in nanometers.

$$\frac{\lambda_{\text{eff}}}{2\pi R} = 13.74 - 0.12[\varepsilon_\infty + \varepsilon_s 141.04]/\varepsilon_s - 2/\pi + \frac{\lambda}{\lambda_p} 0.12\sqrt{\varepsilon_\infty + \varepsilon_s 141.04}/\varepsilon_s, \quad (14)$$

which defines the coefficients n_1 and n_2 introduced in Eq. (1). Thus, the effective wavelength follows from a simple linear scaling of the free-space wavelength λ.

In order to test the developed theory we numerically analyzed two types of optical antennas: a half-wave dipole antenna and a *3-element Yagi-Uda antenna* [15]. The calculations were performed using the semianalytical multiple-multipole (MMP) method [21]. Figure 3(a) shows the spectral response of a half-wave dipole antenna made of a single aluminum rod of length $L = 110$ nm and radius $R = 5$ nm. The spectrum has a peak at $\lambda = 640$ nm. According to the wavelength scaling rule in Eq. (14) (cf. Fig. 2), an effective wavelength of $\lambda_{\text{eff}} = 2L = 220$ nm corresponds to an incident wavelength of $\lambda = 650$ nm which agrees well with the peak position of the spectrum. A half-wave dipole antenna with the same geometrical parameters but made of gold has a computed resonance at $\lambda = 1170$ nm which again agrees very well with the value predicted by Eq. (14). Notice that at the resonance wavelength the near-field intensity evaluated at the ends of the rod assumes its maximum value [Figs. 3(b) and 3(c)].

It is important to stress that a traditional half-wave dipole antenna consists of two segments of length $\lambda/4$ separated by a tiny feedgap. The feedgap is connected to an impedance-matched transmission line ($Z \approx 73 + i42\ \Omega$) and supplies the antenna with current. However, the perturbation introduced by the feedgap is essentially eliminated by impedance matching and hence, an impedance-matched half-wave dipole antenna is analogous to a single metal rod as considered in this example. Two aligned and closely spaced antenna segments of length $\lambda/4$ would represent a strongly mismatched half-wave dipole antenna [7].

The induced current density inside the half-wave antennas considered in Fig. 3 is calculated as $\mathbf{j} = -i\omega\varepsilon_o[\varepsilon(\omega) - 1]\mathbf{E}$, where $\mathbf{E}$ is the local electric field. We find that the current density is described by $j(z) \propto \cos[z\pi/(L + 2R)]$, in agreement with the offset introduced in Eq. (2). The current is nearly 180° out of phase with respect to the exciting field. If we interpret the induced current as a source current we obtain a transmitting half-wave dipole antenna whose radiation resistance is calculated as $R_{\text{rad}} = 2P_{\text{rad}}/I_o^2$, where P_{rad} is the radiated power and $I_o = \pi R^2|\mathbf{j}_o|$ is the source current. For both the gold and aluminum half-wave antennas we calculate $R_{\text{rad}} \approx 3\Omega$.

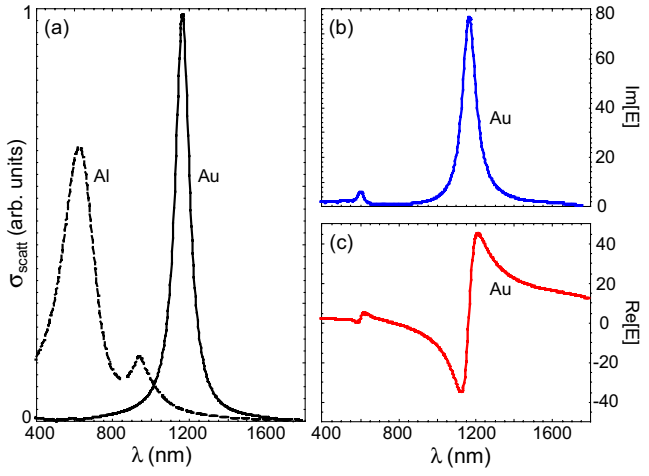

FIG. 3 (color online). Spectral response of aluminum and gold half-wave dipole antennas ($L = 110$ nm, $R = 5$ nm). (a) Scattering cross section of an aluminum rod (dashed curve) and a gold rod (solid curve). (b), (c) Imaginary and real parts of the electric field enhancement evaluated at the poles of the gold rod. The secondary peaks at $\lambda = 940$ nm (aluminum) and $\lambda = 595$ nm (gold) arise from intraband transitions.

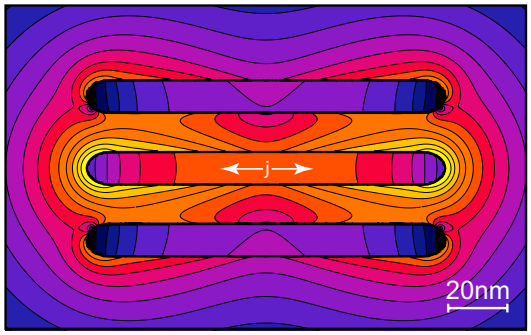

FIG. 4 (color online). Field distribution near a 3-element optical Yagi-Uda antenna consisting of a driven center element ($\lambda = 1150$ nm) and two parasitic elements of equal lengths (E^2, factor of 2 between adjacent contour lines). The parasitic elements increase the antenna efficiency by 65%.

Gold nanorods have been synthesized by colloidal chemistry by various groups and aspect ratios larger than 10:1 have been reported [22]. Let us consider a gold nanorod with $R = 5$ nm and aspect ratio 8:1 ($L = 80$ nm) suspended in a solution with $\varepsilon_s = 1.72$ (H_2O). The fundamental resonance is then expected to be found for $\lambda_{\text{eff}} = 2L = 160$ nm. According to Eq. (13) this value corresponds to a wavelength of $\lambda \approx 1180$ nm, which agrees with the measurements by Yu *et al.* [22]. Monopole antennas exhibiting a $\lambda/4$ resonance have been recently investigated by Taminiau *et al.* [4]. For a $R = 20$ nm aluminum rod excited with $\lambda = 514$ nm the resonance length was found to be $L \approx 75$ nm, from which one derives $\lambda_{\text{eff}} \approx 300$ nm. The value derived from our theory is slightly larger ($\lambda_{\text{eff}} = 320$ nm) which can be attributed to the fact that $L \not\ll 4R$ and that the antenna considered by Taminiau *et al.* is not located above perfectly conducting ground.

The here developed wavelength scaling can be applied to more complex antenna designs, such as antennas with parasitic elements, self-scaling antennas, or phased arrays. In Fig. 4 we consider a simple 3-element optical Yagi-Uda antenna made of a driven antenna segment (center) and two parasitic antenna segments of equal lengths. The driven element ($L = 110$ nm, $R = 5$ nm) is fed by an impedance-matched source current with frequency $f = c/\lambda$, where c is the vacuum speed of light and $\lambda = 1150$ nm. The phase of the induced currents in the parasitic elements can be influenced by the length of the elements and by their spacing. In the simple example shown in Fig. 4 the parasitic elements increase the overall antenna efficiency by 65%; i.e., for the same source current the emitted power increases by a factor of 1.65. The Yagi-Uda antenna can be optimized for efficiency and directivity by calculating the mutual impedances between pairs of antenna segments and using established design rules [15,23].

In summary, we have derived a linear wavelength scaling rule which makes it possible to downscale established antenna designs into the optical frequency regime. Optical antenna design can be further guided by use of the "lumped circuit" concept introduced recently by Engheta *et al.* [24]. Optical antennas are likely to be employed for boosting the efficiency of light-matter interactions in a wide range of settings, such as photovoltaics and light-emitting devices.

I would like to thank Palash Bharadwaj, Sergey Bozhevolnyi, Tim Taminiau, and Miguel Alonso for fruitful discussions and valuable input. This work was supported by the Air Force Office of Scientific Research MURI (Grant No. F-49620-03-1-0379).

*http://www.nano-optics.org

[1] D. W. Pohl in *Near-Field Optics, Principles and Applications*, edited by X. Zhu and M. Ohtsu (World Scientific, Singapore, 2000), pp. 9–21.
[2] J. N. Farahani, D. W. Pohl, H. J. Eisler, and B. Hecht, Phys. Rev. Lett. **95**, 017402 (2005).
[3] P. Anger, P. Bharadwaj, and L. Novotny, Nanotechnology **18**, 044017 (2006).
[4] T. H. Taminiau *et al.*, Nano Lett. **7**, 28 (2007).
[5] H. G. Frey, S. Witt, K. Felderer, and R. Guckenberger, Phys. Rev. Lett. **93**, 200801 (2004).
[6] P. J. Schuck *et al.*, Phys. Rev. Lett. **94**, 017402 (2005).
[7] P. Mühlschlegel *et al.*, Science **308**, 1607 (2005).
[8] H. Mertens *et al.*, Nano Lett. **6**, 2622 (2006).
[9] D. Derkacs *et al.*, Appl. Phys. Lett. **89**, 093103 (2006).
[10] K. Okamoto *et al.*, Nat. Mater. **3**, 601 (2004).
[11] S. A. Choulis, M. K. Mathai, and V. Choong Appl. Phys. Lett. **88**, 213503 (2006).
[12] E. Cubukcu *et al.*, Appl. Phys. Lett. **89**, 093120 (2006).
[13] J. Aizpurua *et al.*, Phys. Rev. B **71**, 235420 (2005).
[14] E. K. Payne *et al.*, J. Phys. Chem. B **110**, 2150 (2006).
[15] T. Milligan, *Modern Antenna Design* (McGraw-Hill, New York, 1985).
[16] C. Fumeaux *et al.*, Infrared Phys. Technol. **41**, 271 (2000).
[17] F. Neubrech *et al.*, Appl. Phys. Lett. **89**, 253104 (2006).
[18] D. B. Rutledge, S. E. Schwarz, and A. T. Adams, Infrared Phys. **18**, 713 (1978).
[19] We consider the effective wavelength for the lowest-order (dipolar) resonance. For higher-order resonances the offset $4R$ needs to be scaled as $4R/N$, with N being the order of the resonance.
[20] M. Abramowitz and I. A. Stegun, *Handbook of Mathematical Functions* (Dover, New York, 1965).
[21] L. Novotny and B. Hecht, *Principles of Nano-Optics* (Cambridge University Press, Cambridge, England, 2006).
[22] Y.-Y. Yu *et al.*, J. Phys. Chem. B **101**, 666 (1997).
[23] R. E. Collin and F. J. Zucker, *Antenna Theory* (McGraw-Hill, New York, 1969).
[24] N. Engheta, A. Salandrino, and A. Alu, Phys. Rev. Lett. **95**, 095504 (2005).
[25] P. B. Johnson and R. W. Christy, Phys. Rev. B **6**, 4370 (1972).
[26] D. Y. Smith, E. Shiles, and M. Inokuti, in *Handbook of Optical Constants of Solids*, edited by E. D. Palik (Academic, New York, 1985), p. 369.